Imaging and reconstruction of positive streamer discharge tree structures

Imaging and reconstruction of positive streamer discharge tree structures

To cite this article: Siebe Dijcks *et al* 2023 *Plasma Sources Sci. Technol.* **32** 045004

OPEN ACCESS
IOP Publishing
Plasma Sources Science and Technology
Plasma Sources Sci. Technol. **32** (2023) 045004 (13pp)
https://doi.org/10.1088/1361-6595/acc821

Imaging and reconstruction of positive streamer discharge tree structures

Siebe Dijcks, Martijn van der Leegte and Sander Nijdam*

Eindhoven University of Technology, Eindhoven, The Netherlands

E-mail: s.nijdam@tue.nl

Received 30 January 2023, revised 15 March 2023
Accepted for publication 28 March 2023
Published 11 April 2023

Abstract

Streamer discharges often exhibit branching, which can greatly affect their behavior and will lead to so-called streamer trees. In this work we present a methodology for investigating the structure of a streamer discharge tree by means of advanced imaging techniques. Stereoscopic and stroboscopic techniques augment the images with depth perception and temporal information relevant to study the inherently stochastic three-dimensional and transient streamers. A semi-automated post processing algorithm is developed to make a reconstruction of the streamer discharge tree formation. This results in a tree of streamer segments, separated by branching events, where velocities, diameters and trajectories are used to characterize the morphology. The workings of the algorithm is detailed using an exemplar measurement series of positive streamers in synthetic air at 233 mbar.

Keywords: streamer, branching, advanced imaging techniques, stereoscopy

(Some figures may appear in colour only in the online journal)

1. Introduction

Streamers occur when strong local electric fields ionize a dielectric gaseous medium enough to create a conductive plasma. The curved space charge layer at the front of this expanding plasma can maintain the strong electric field, thereby allowing it to propagate, roughly along the external field direction. This is what causes long filamentary conductive channels, streamers, to form. Good reference on the physics of streamer discharges are Nijdam *et al* [1] and the references therein. Local perturbations in the leading edge space charge layer, caused by the stochastic production of electron avalanches, can grow into branching events [2–5]. These branching events determine to a large degree the morphology of the streamer discharge tree, which is the focus of this work.

Streamer discharges can be found in high voltage equipment, where they can form unwanted short circuits and damage the equipment. On the other hand, streamers contain a non-equilibrium and transient plasma in their heads, which can be beneficial for generating highly energetic species for gas treatment applications [6].

In this paper we will look at imaging as a diagnostic tool for investigating the stochastic and filamentary propagation of streamers and how its morphological features affect the plasma properties of the streamer. While the imaging of streamers is an established technique to investigate the relevant physical processes [7, 8], the extra spatial and temporal detail achieved in this work, together with the amount of data which can be processed, will shed more light on the behavior of these discharge phenomena. The goal is to use experimental results of streamer characterizing parameters (velocity, diameter and orientation) in a direct comparison to validate modelling efforts of three dimensional streamer morphologies, like in the early works of Gallimberti [9] to the more recent work by Marskar [10] and the group of Teunissen and Ebert [3, 11, 12], where for the latter the experimental data presented in this work is used to make the comparison between experiment and

* Author to whom any correspondence should be addressed.

simulation. In [13] we compared results for cylindrically symmetric single streamers, made in an identical setup but at different conditions of gas pressure and applied voltage. These comparisons show good agreement of the simulations with the experiment when boundary and initial conditions are properly matched.

In this work, the methodology for capturing and analyzing the morphology of more complex streamer discharges is outlined in detail. The discharge morphology is investigated by creating full 3D spatial and temporal reconstructions of single voltage pulse discharge events. In the following section 2, the experimental setup developed for generating streamer discharges and imaging them, is explained. Section 3 briefly discusses the streamer branching theory and how the parameters relevant to this can be extracted from the image. The imaged discharge trees are then reconstructed with post processing using an algorithm which is described in steps in section 4. The output of this reconstruction is the velocity, diameter and orientation of all the streamer trajectory segments, which are split up by its branching events. The results for an exemplar measurement series in synthetic air are presented and discussed in section 5. Finally the article is concluded and an outlook is given in the final section 6. The raw and processed data togther with the MATLAB scripts are available in the online zenodo repository .

2. Experimental setup

Since streamer discharges are a reaction of a gaseous medium to strong electric fields, having good control over both the applied electric field distribution and the gaseous medium inside the discharge volume is crucial. In this work, the scope is limited to positive primary streamers, i.e. the initial streamer and its forked branches originating from a positively charged electrode and which are propagating against the electric field direction. The experimental setup (schematically shown in figure 1) is designed to create streamer discharges in widely varying conditions of gas composition, pressure and applied voltage pulses. The streamer morphology, which is strongly dependent on these conditions, can than be tuned for certain morphological features and complexities, which can then be resolved by the post processing algorithm.

The operable pressure range to create streamer discharges in this vessel is 10–1000 (233) mbar in the media of nitrogen and carbon dioxide with any amount of oxygen admixed (most notably forming synthetic air) with a discharge gap of 1–15 (10) cm; the values in parentheses are for the results presented in this paper.

The streamers are generated between two opposing disk electrodes, which leads to a somewhat homogeneous electric field between them. There is a small protruding needle (10 mm protrusion, 1 mm diameter and 60° tip angle) from the powered electrode, which locally distorts this field homogeneity, and thereby helps to initiate the streamer at a well defined point in space while reducing the inception voltage and jitter. Applying a voltage pulse with a fast rise time to the protruding needle with a slightly overvolted gap gives a well defined streamer discharge inception in time and ensures that most pulses result in a discharge.

The discharge volume between the electrodes is radially centered inside a stainless steel vacuum vessel, which together with the bottom grounded plate is electrically grounded, see figure 1 for the dimensions. The vessel is nearly cylindrically symmetric, except for further away from the central axis where the optical windows break this symmetry, see also figure 2. The vessel is connected to a vacuum pump through a control valve to regulate the pressure, and to the gas cylinders through a flow controller to control the flush rate, which in this work is $2\,\mathrm{sl\,min^{-1}}$. Depending on the pressure it takes a few minutes for all the gas in the vessel, approximately 100 l, to be replenished. For the streamer discharges in air, a synthetic air mixture of nitrogen (80%) and oxygen (20%) at a purity of >99.999% is used.

The voltage waveform is created by discharging a capacitor through a push pull voltage switch (Behlke HTS 651-15-SiC-GSM) at 20 voltage pulses per second (pps). The voltage pulse-width and repetition rate are variables controlled by the switch, the amplitude by the charging voltage of the high voltage power supply and the rise and fall times by the complete circuit properties. An example of the voltage waveform is shown in figure 1. The 200 Ω resistor is there to limit the short-circuit current, prevent a streamer-to-spark transition and protect the switch. In addition, the voltage pulse width is set to the time that the streamer needs to cross the gap, so that when the gap is shorted by the streamer the pulse ends and a large increase in current associated with a spark is prevented. The 3 MΩ charging resistor protects the high voltage power supply from excessive load. The current and voltage characteristics are measured at the powered electrode on top of the vessel by a current (Magnelab CT) and a high voltage (North Star PVM) probe.

The light imaged by the system originates for >98% from the second positive system (SPS) of molecular nitrogen at around 330 nm [14]. The rest of the emission is mainly first positive and first negative emission of molecular nitrogen. The volume between the disk electrodes is imaged through a large quartz window by an intensified charge-coupled device (ICCD) camera (Lavision PicoStar HR + UV photocathode) with a 105 mm lens which can be fully gated at frequencies up to 100 MHz. The resolution of the CCD is 1 MP, but due to the intensifier, the effective resolution is a little lower than a quarter of that. Therefore, the raw images are binned 2×2 without loss of effective resolution. For the imaged 10 cm discharge gap, the spatial resolution is around 0.4 mm. A prism with reflective coating together with two mirrors are used to create a stereoscopic image on the ICCD (see figure 2), the distance between these mirrors and the discharge volume determines the angle between the stereoscopic perspectives, which in this work is 29° and is limited by the size of the large quartz window. Larger angles, up to 90°, produce a more accurate depth estimation, but make it more difficult to match similar features in the resulting stereoscopic images.

The triggering and modulation of the discharge and camera inputs are performed by a function generator (Keysight 33600A), where the first output is used to trigger the push

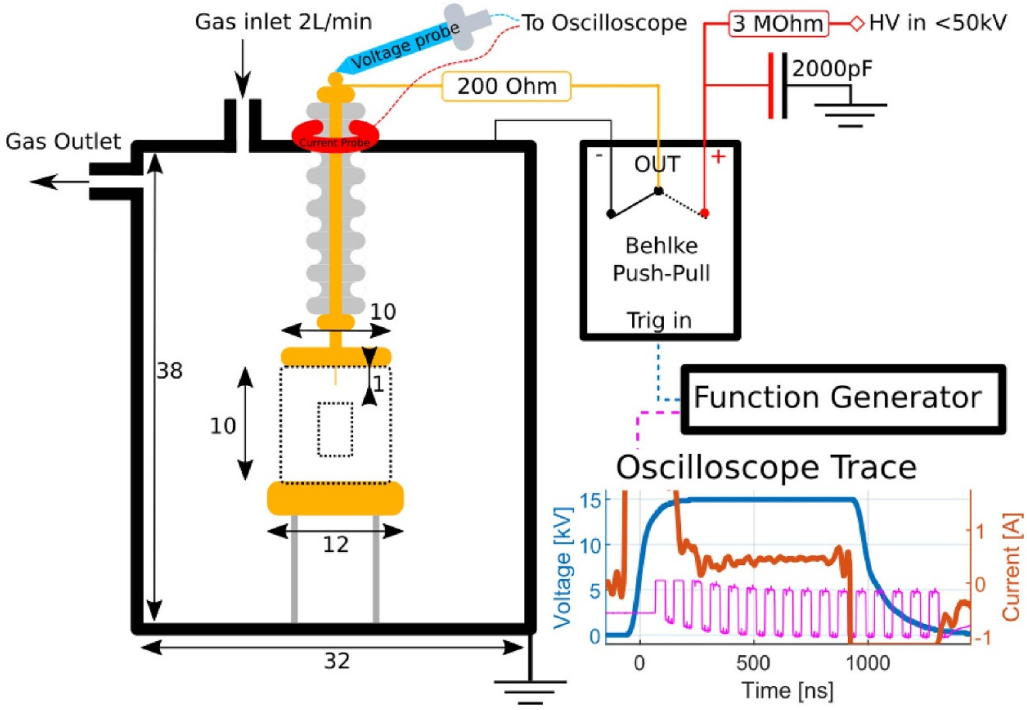

Figure 1. Schematics of the experimental setup. The brass and copper electrodes are colored gold. Depicted dimensions of the vessel and electrode geometry are in centimeters. The oscilloscope trace shows the current and voltages measured atop the vessel. The current scale is adjusted to emphasize the low current flowing during the streamer propagation instead of the high capacitive current peaks at the voltage edges. The magenta pulse train is the gate for the ICCD camera used to create the stroboscopic effect in the images. The dotted lines between the opposing disk electrodes depict the field of view for figures 3 (smaller rectangle) and 5(a) (larger rectangle).

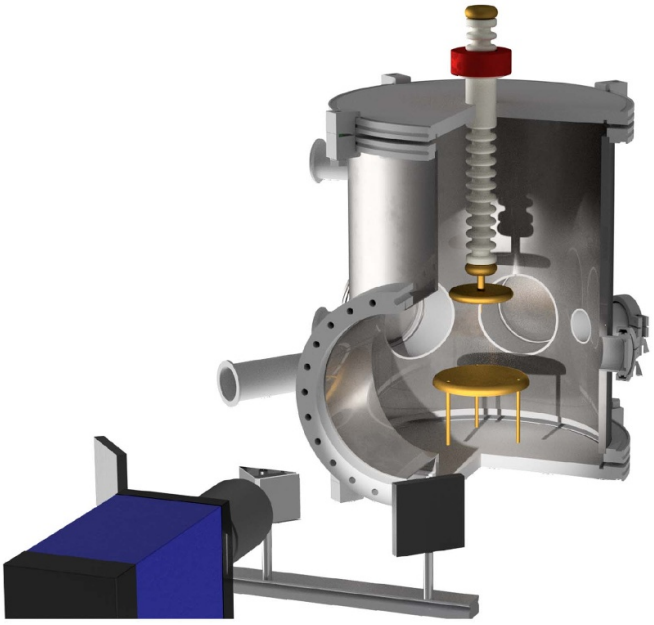

Figure 2. Schematic render of the vessel together with the ICCD camera observing the discharge region through the stereoscopic optics. The prism has reflecting sides, acting as a symmetric mirror. The outer mirrors can be individually rotated to project both stereoscopic perspectives on different areas of the ICCD which creates the composite image like shown in figure 5(a).

pull switch and the second to directly gate the intensifier of the camera. Stroboscopic techniques have been used before to image the very transient development of streamers, see for example Pancheshnyi *et al* [7] and Trienekens *et al* [15]. The stroboscopic pulse train is chosen such that there is a clear separation between the exposures of the streamer head on the captured image. The radiative lifetime of the nitrogen excited by the streamer head in the gas limits the maximum exposure frequency. With an electrode gap of 10 cm and streamer velocities of about 5×10^5 m s^{-1}, and thus a propagation

time of generally around 200 ns, we found that gate repetition frequencies of 8–40 MHz give the best results. This frequency is used with a duty cycle, which controls the electronic shutter opening and closing, set to 50% for the results presented in this work, with the exception of the stroboscopic images of figure 3. The number of pulses in the train is adjusted such that the full propagation of the streamer is visible in the discharge gap. A few extra pulses are added to the start and end of the train to make temporal alignment easier, these few pulses outside of the voltage pulse do not accumulate any significant extra light onto the image. An example of the gating signal of the camera is shown in figure 1

While the gating of the ICCD is very fast, the actual repetition rate for imaging is not. The triggering of the CCD is completely separate from the intensifier, and runs at its maximum frame rate per second (fps) for the chosen settings, which is 7.22 fps; i.e. it takes 139 ms to capture an image and transfer it to the PC. This means that the discharges repeating at 20 pps are sampled by the imaging system at 7.22 fps, such that roughly one in three discharges is captured.

3. Streamer features

The goal of the image processing algorithm is to reconstruct the discharge tree morphology in the highest possible detail. In this section, the imaged discharge features, how they relate to the morphology and how they are interpreted, especially regarding the branching, are discussed.

The detected feature is the front of the streamer discharge, where the strong local electric field has accelerated the electrons which ionize the space charge layer region. In addition to ionizing, electron impact reactions create the upper state species for SPS emission ($C^3\Pi_u \rightarrow B^3\Pi_g$), from the N_2 ground state present in the gaseous medium. This radiating volume associated with the curved space charge layer is captured by the camera. The captured images show this layer, elongated along the propagation direction due to the camera gate, streamer velocity and effective lifetime of the SPS, which results in the characteristic nearly hemispherically shaped features on the images, see figure 3. By combining the stereoscopic and stroboscopic techniques to image the discharge, extra spatial and temporal information is captured compared to a standard 2D image or a non-stroboscopic stereo image like used by Nijdam *et al* [16]. This results in two, side by side discharge trees, where the streamer paths are temporally sampled by the stroboscopic pulse train, see figure 5(a).

Before, we mentioned that the morphological complexity of the streamer discharge can be tuned using the experimental setup, here the considerations made for this tuning are detailed. General theory on the behavior of streamers can be found in the book of Raizer [17] and the more recent reviews of Nijdam *et al* [1] and Babaeva and Naidis [18]. When a strong positive electric potential is applied to a gaseous medium, the streamer discharge, specifically the region of high E/N, can ionize the medium and extract the free electrons through the streamer channel. The speed of this process is directly related to the magnitude of the applied potential distribution, which governs the diameter and velocity of the streamer head. In the absence of branching, there is a positive correlation between the amplitude of the applied voltage waveform and the streamer diameter and velocity. Similarly there is a negative correlation between the pressure and the streamer diameter and velocity when all other conditions are kept identical. The smaller the diameter of the streamer head, the smaller the volume of high E/N is. In Briels *et al* [19] the minimum diameter, with which a streamer can propagate at various pressures is investigated and the similarity laws for scaling these parameters are proposed. We have numerically investigated the behavior of a single non branching streamer in Li *et al* [13] by comparing to streamers created in the experiment described in section 2. Another critical parameter for the morphology of streamer discharges is the ratio of its diameter compared to its length (L/D). High ratios ($\gg$10) are more likely to laterally drift and branch, since they propagate relatively much further, Luque and Ebert [20] mentions a ratio of distance between branching events over the streamer diameter of about 8, the results of this work are presented in section 5 and specifically figure 10.

The stability of the streamer head during propagation, which determines the branching rate, is affected by both stabilizing and destabilizing processes. The high E/N region and thus ionization rate at the pole of the hemispherical layer is strongest, focusing and stabilizing the streamer along its axis. However, stochastic variations in the curved space charge layer, due to for example the streamer directed avalanches produced by photo ionization, can cause local charge gradients. These charge gradients lead to local maxima in the electric field, which can then each sustain their own local ionization maxima and propagate into that direction, resulting in a branching event. The field maxima for both local charge maxima, which share the same polarity, will point away from each other, resulting in deflecting trajectories of the daughter streamers sprouting from the branching event. In Luque and Ebert [2] the creation of 3D discharge trees are modeled, and Bagheri and Teunissen [3] looked into the effects of stochastic photoionization when modelling streamers in 3D.

In figure 3 the stroboscopically imaged trajectories of five propagating streamers in separate discharges but identical conditions are shown. The various levels of deformation in the streamer head during the branching events are clearly visible. In figure 3(d) the centers of the streamers are marked with green dots, and the boundaries of the imaged streamer heads in dashed teal lines. These markings give an indication of what the algorithm will be able to work with. Through the green dots the trajectories are drawn, and special distinction is created between the incoming streamer, the parent (solid green), and the outgoing streamers, the daughters (dashed green). Around the branching point, two possible trajectories of the branched streamer are presented. The white triangle marks the perturbation of the streamer where a second local maximum in intensity, within what can be considered the same streamer head, is used to draw an alternative trajectory. Within the simplification of describing the propagating streamers by assigning trajectories, any trajectory between the two sketched cases is valid. In reality however, the streamer head is a complex problem where the space charge distribution is perturbed around the branching event, and with the current imaging

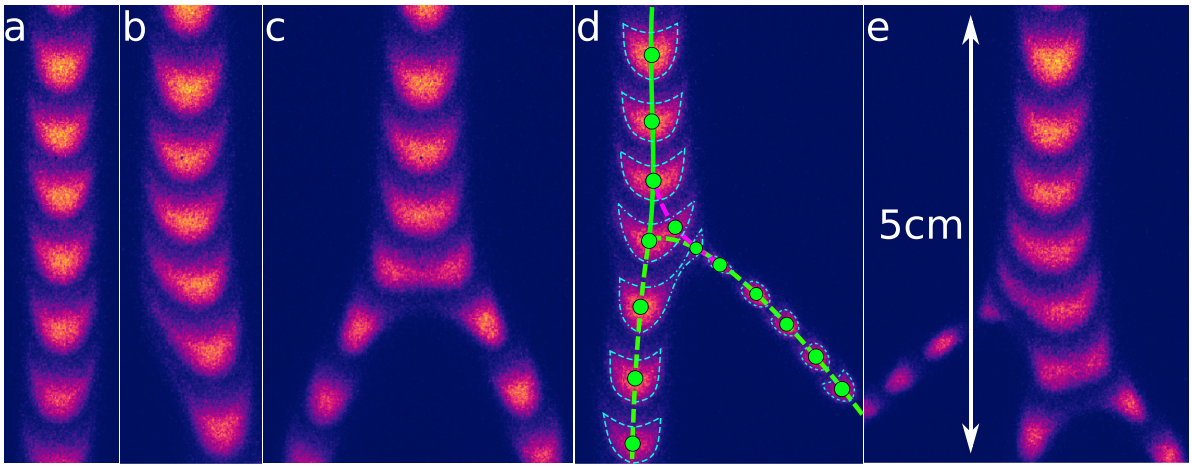

Figure 3. False color images showing the branching variations. (a) Single unperturbed streamer, (b) slightly deflecting but not branching streamer, (c) streamer branching symmetrically, (d) streamer branching non-symmetrically, with annotations marking the circumference in dashed teal and detections linked by trajectories in green, and (e) more complex variation of the previous two. Images are captured from the center of the discharge gap, see the smallest dashed circumferences between the electrodes in figure 1. Discharge conditions are 150 mbar air at 20 kV, with stroboscopic gates of 10 ns at 30 MHz.

diagnostics the exact point where the distribution goes from a single maximum to multiple maxima (the branching event) is impossible to determine. A parameter with which to quantify these branching events is the branching angle [4, 16, 21]. This angle is defined between the daughter streamers and will be used in this work as well.

The addition of O_2 to pure N_2 (like in air) causes photoionization, which reduces the stochasticity and therefore branching compared to a discharge in pure nitrogen [1], see figure 4. In this figure there are many arrested streamers, which stop shortly after they branch [22]. The large amount of branching gives a lot of complexity to the discharge tree, which makes it too cluttered to resolve with the algorithms described in this work.

In this paper, the focus is on the morphology of the streamer discharge tree, but this morphology also significantly affects the plasma created at the heads of the propagating streamers. The gaseous medium locally experiences a strong and transient electric field pulse when the streamer passes through. In the work of Babaeva and Naidis [18], Naidis [23] and our own work [24] this relation between the electric field distribution and the streamer properties like diameter and velocity are investigated. The velocity and curvature of the streamer head directly dictate the electric field magnitude profile experienced by the gaseous medium. Both properties are strongly affected by branching, especially during a branching event. See again figure 3, where the diameters and velocities (which are proportional to the distance between captured exposures) of branching streamers fluctuate significantly. Therefore this would lead to significantly differently treated volumes of gas along the streamer trajectories.

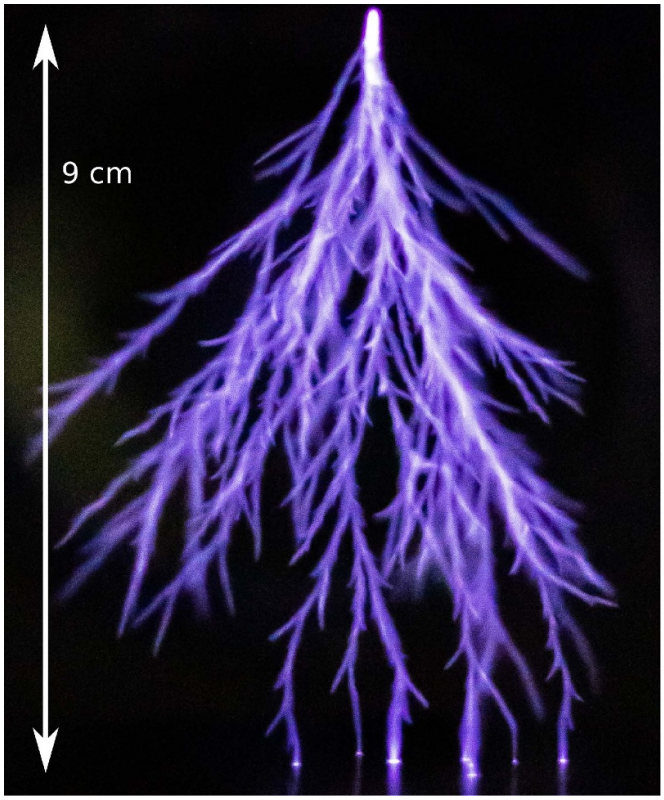

Figure 4. CMOS image of a streamer discharge in pure N_2 at 200 mbar and 20 kV—1 μs voltage pulse at a 1 pps repetition rate. The discharge gap is strongly overvolted for this image to make the streamer discharge tree bright enough to be captured by the CMOS camera (Sony alpha 7 Mark III). Color in image is corrected from a more blueish hue to purple to reflect the live perception.

4. Reconstruction algorithm—post processing

In order to categorize the frequency and angle of branching events that the streamer undergoes, an algorithm is designed around finding these branching events and their in- (parent) and outgoing (daughter) streamer trajectories. The purpose of the reconstruction algorithm is to transform the raw image, figure 5(a), into a 3D spatially and

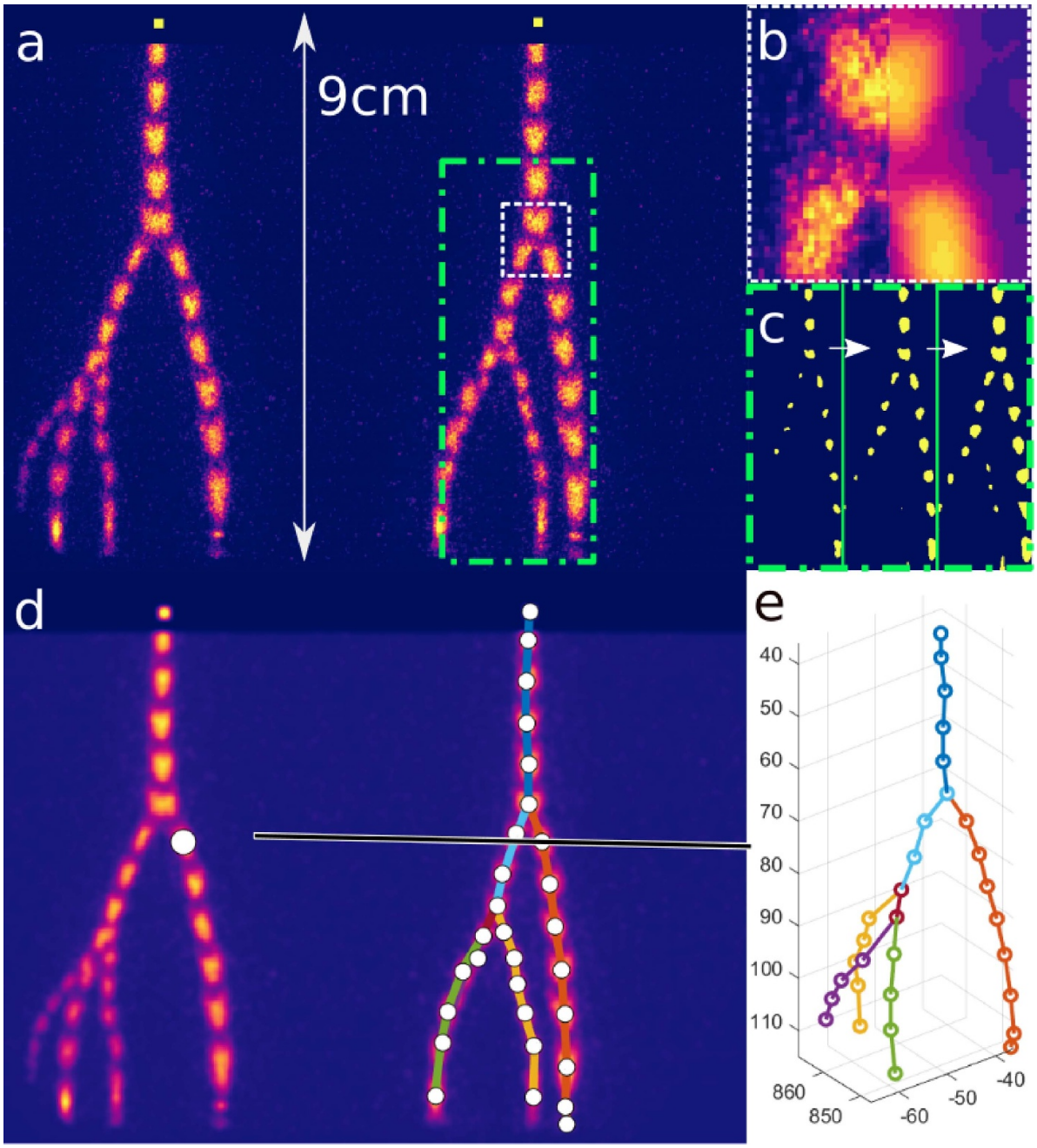

Figure 5. Steps in the image reconstruction process: (a) original image captured by the ICCD, displayed in false colors, (b) zoom of original on the left to processed (Gaussian blurred and k-means clustered) on the right, (c) binary images of the 12th through 10th layers of the right hand stereoscopic view, note the extra detected blobs for the lower layers, (d) detected blobs, segments and epipolar line, and (e) 3D reconstruction with colored segments. Axes are in millimeters, where the origin (0,0,0) mm is the position of the virtual stereoscopic left camera.

temporally resolved streamer discharge tree, as is depicted in figure 5(e).

The first step is to detect the individual blobs caused by the multiple exposures of the streamers in each image. For single streamers, like depicted in figure 3, this is trivial, however for more complex streamer discharge trees, and especially near branching events, this poses many challenges and will not always work. This is true for both the semi-automated algorithm as well as for a manual inspection of the images around branching events.

The initial step in the detection is to apply a Gaussian blur to the image followed by k-means clustering [25] of the pixel intensities. This is to simplify the image and prepare it for binarizing, while minimizing loss of information. The Gaussian blur spatially averages the pixel intensities and the k-means clustering algorithm clusters the local intensities together to generate an image with only 14 pixel intensities (the value of 14 is arbitrarily chosen for best performance and can be varied for different experimental conditions), from originally 4096 intensities (12 bit image depth), see figure 5(b). The

14 k-means layers (intensities) are stored as separate binary images.

For each of the binary k-means images, the blobs are then segmented, analyzed and the valid connected components are labelled using the MATLAB image processing toolbox workflow. Setting the thresholding values in the binarizing filter is the first of two manual steps in the semi-automated algorithm. However, for images created at similar experimental conditions this setting can be fixed. The connected pixels (adjacent true pixels) forming the blobs represent the exposures of the streamers. This analysis is started from the top k-means layer (only containing the brightest centers of blobs), such that for each underlying k-means layer only new detections of fainter blobs are added, see figure 5(c). Existing blobs, positioned over blobs labelled in the previous layer are assigned to their parent blob, while merging blobs are ignored (for the lowest k-means layer practically all blobs have merged into a large blob representing the streamer tree silhouette, see the outer silhouettes in figures 5(b) and (d)). All coordinate centers, determined as the center of mass of the detected blobs in their highest k-means layer for both stereoscopic views are stored.

Correlation of the two stereoscopic images is performed using the epipolar line [26], which follows from the geometry in stereoscopic vision. This means that the center of a detected blob on one stereoscopic view represents a line in the other view, see figure 5(d). The detected blob center and the best matching blob from the other stereoscopic view where the epipolar line crosses through are now paired. This procedure is trivial for many blob pair detections, but can be very difficult immediately after branching events and when streamers cross behind each other in one view. Therefore, this step is generally automated, but for the most difficult situations (those with competing options) the algorithm prompts for user input using a simple intuitive user interface (UI) to assign the proper correlation, this is the second manual step in the algorithm.

The 3D coordinates are triangulated using the intersection of both stereoscopic epipolar lines. Using the fundamental matrix we now relate the pixel positions of both stereoscopic views to real world coordinates. This matrix is acquired using the stereo camera calibration toolbox in MATLAB. To construct this matrix, it analyses a few dozen images of checkerboard patterns with known dimensions placed within the discharge volume.

Next, for all points in 3D a cost matrix is calculated from their mutual Euclidean distances. From this cost matrix, a directed graph (streamers propagate from the top powered needle downwards) for all possible connections is constructed using the graph and network algorithms toolbox in MATLAB. Shortest path and minimum spanning tree optimizations are applied to clean up the number of connections to achieve the most realistic streamer paths. Figure 5(e) shows the final 3D streamer tree with all the triangulated detections for the original image of panel (a). Branching events divide the paths into segments depicted by the various colors.

For some segments, confirmed blob pairs are missing near branching events, due to overlapping streamer branches in one of the camera views. Some branching events can cause significantly reduced streamer diameters, intensities and velocities for one or both of its daughters. When such a branching event is imaged, the reduced velocity can cause the stroboscopically captured exposures to start overlapping (the stroboscopic gating frequency is fixed for a measurement series, optimized to capture most streamer segments, except near branching events), while due to the reduced diameter and intensity the blobs can fade below the detection threshold. For these scenarios it is more difficult to assign blob pairs with the limited image resolution and contrast available. In figure 3(d) it is clearly visible that the streamer segment branching away from the original path has a significantly reduced propagation velocity (detections are closer together) and diameter during and directly after the branching event. In the non-zoomed stereoscopic images, such detailed features around branching events are lost, see the second and third branching events in figure 5, where the purple, green, and yellow sections in figure 5(e) have their origin. Especially in the right side stereoscopic view of figures 5(a) and (d), in addition to two branching events taking place very near each other, there are two segments which are almost completely overlapping in one of the stereoscopic views. The segments are still mostly resolved, but the purple and yellow segments are poorly connected to their parent segments in figure 5(e).

To improve the reconstruction of the full streamer tree, the segments around a branching event are fitted. These fits are made in a 2D branch plane, constructed from the parent and daughter segments for each specific branching event. The streamer blob pairs of the participating segments nearest to the branching event are given extra weight when fitting this plane. Figures 6(a) and (b) depict the branch plane, spanned by vectors $\vec{u}$ and $\vec{v}$ for the last branching event of the streamer tree. For these fits it is assumed that the three segments participating in the branching event lie on a 2D plane, which generally works very well, except for the lower part of the streamer tree and for the longest segments, where the streamers curve towards the grounded plate, and thus out of the branch plane. This, however, has little effect on the reconstruction around the branching event. See figures 6(d), 8(a) and 9 for an overview, where the triangulated detections are marked in green and the segments in the branch planes are rendered as colored tubes. The velocity of a segments, the color of the rendered tube, is the mean velocity of the segment and the diameter of the rendered tubes are determined from the detected blobs (see below for more details).

The paths of the parent and daughter streamers are fitted to the measured detections with circular trajectories. This means that the path is determined only by the orientation of the streamer and an origin, where the orientation compromises of two terms: its initial value, which is the branching angle, and the curvature of the segment. The velocities are assumed constant for each segment and are determined from the Euclidean distance between the detections in 3D and the stroboscopic pulse train frequency. The origin for the first segment is located at the needle tip, and for all successive segments it is fitted along its parent segment, and this branch point along the parent trajectory is the third fitted variable for the circular

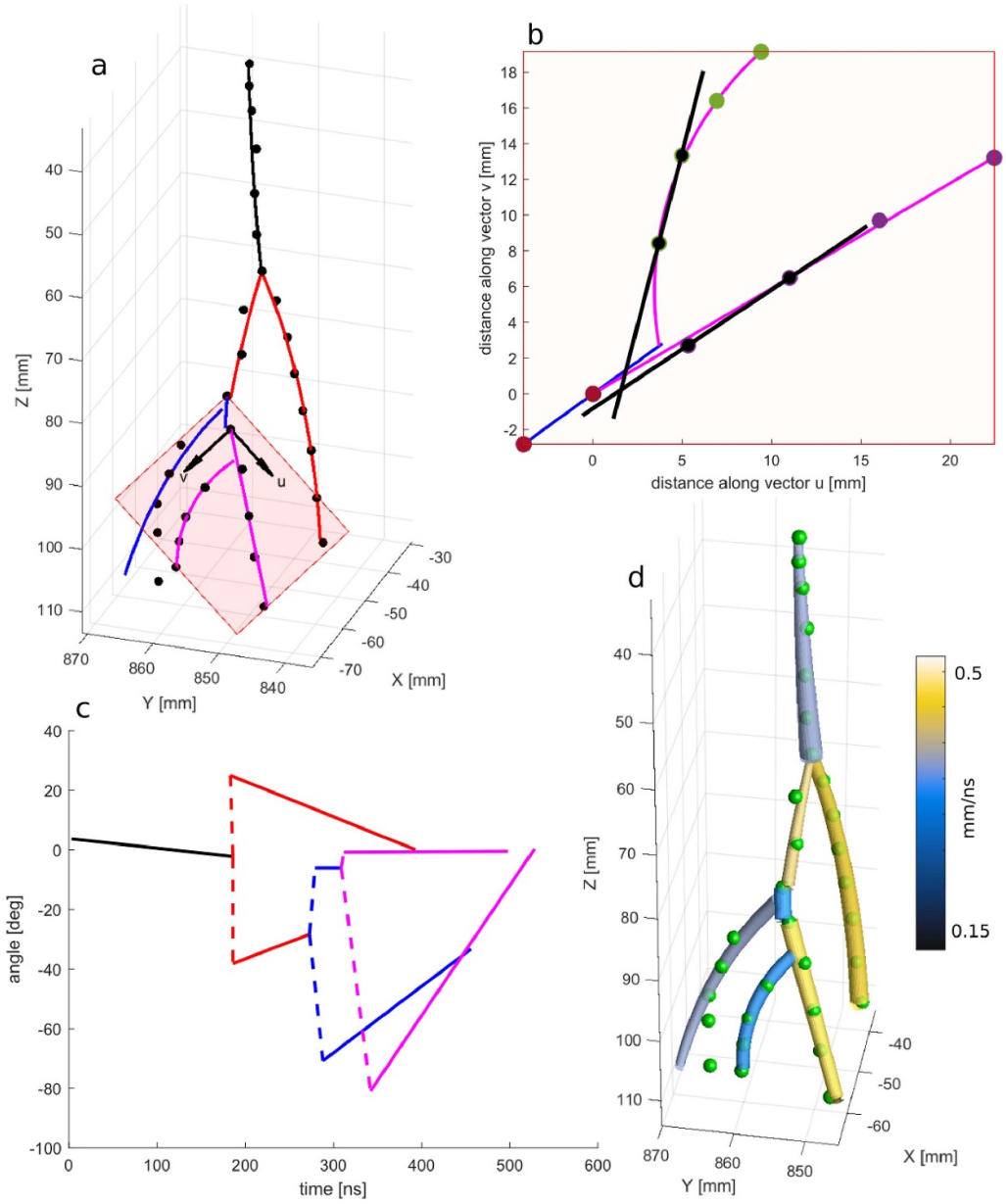

Figure 6. Steps in the streamer trajectory analysis: (a) 3D triangulated points with fitted trajectories, branch plane of the last branching event in red, with its basis vectors $\vec{u}$ and $\vec{v}$ indicated, (b) circular trajectory fit through detected points projected to the branch plane, with annotated on top in black the simplified angle determination by linear trajectories, (c) cumulative branching angles from successive branch events. The segments are straight curves due to the circular trajectory assumption, the steepness indicates the curvature of the trajectory. The dashed lines indicate the change in orientation of the daughters compared to their parent within the branchplane. Note that the different colored lines are from different branch planes spanned by different vectors, so absolute angular values cannot directly be compared from this plot. (d) The final fitted trajectories rendered as tubes with radii derived from the streamer detections FWHM and colored according to their mean velocity. The original triangulated detections are plotted as green dots.

trajectories of the daughters. This also means that the origin of both daughter streamer trajectories can be at separate points along their shared parent streamer trajectory. The advantage of this method is that each segment can thus be fitted by only three variables, each of which has a direct significance to the streamer morphology. Figure 6(b) shows an example of these fitted trajectories and in figure 6(c) the angle and curvature of each trajectory of the branching events are depicted for the entire streamer tree. The advantage of fitting the segments is that the branching angles are very well resolved and missing detections are not as significant since the entire segment is fitted and can therefore be extrapolated to the missing detections. However, information about rapid variations in direction, velocity and diameter directly after a branching event are averaged out by this method. The missed detections also impaired the temporal synchronization of the streamer segments, but by fitting the daughter trajectories to the parent trajectory all streamer branches are also temporally synchronized, resulting in the full spatio-temporal reconstruction of the trajectories.

In order to make a comparison also a linear trajectory method for determining the branching angle is included, see the black lines in figure 6(b).

The diameter of the streamer paths at the detection points is determined by taking a fitted Gaussian full width at half maximum along the cross section of the detected streamers in the original image perpendicular to the propagation direction. In figure 6(d) a full 3D render of the streamer trajectories together with the detections (blob pairs) is shown.

5. Results and discussion

The streamer discharge reconstructed in figures 5 and 6 is the 29th out of a measurement series of 128 images shot in one take, taking the final remarks of section 2 into account. In order to see how successive discharges affect each other, we have analyzed the number of branches in each image of this series and plotted these in figure 7. This is related to work by Chen *et al* [27] who performed a more extensive analysis of shot to shot discharges in a similar experiment. Our results show that discharges with inception appear in clusters (even though only about one third of the discharges is imaged), but the streamer length and branch number seem randomly distributed. From this, we can conclude that leftover species from previous discharges do affect the inception probability but hardly affect the exact streamer morphology for our conditions. While generally the streamers incept at the beginning of the voltage plateau of the waveform, some streamers incept towards the end of the applied pulse, which causes their propagation to be cut short by the voltage pulses falling edge. For work on inception related delay times in synthetic air see Mirpour *et al* [28].

In figure 8, the reconstruction of the 30th streamer of the series is visualized. This is one of the more complex streamer trees which our method is still able to fully resolve.

There are multiple possible reasons why discharge images cannot be fully resolved into streamer trees. This can be the case when there is too much overlap between trajectories in one or both of the stereoscopic views. Overlapping trajectories can be resolved up to a certain degree, but for excessive overlap the reconstruction fails. This is generally the case for the most complex of streamer trees containing many branching events and thus trajectories. Especially when branching events appear close together, daughter streamers can become indistinguishable and merge into a large blob, which also affects the diameter determination. This can bias the overall statistics of a measurement set towards the simpler trees when these most complex of streamer trees are completely omitted from the data set. Another reason for poor reconstruction are very faint and or very slowly propagating streamers. The usually spaced out detections then merge into a single elongated blob, or the intensities are below the detection threshold, preventing accurate detection and reconstructions of the trajectories. This can lead to another bias, this time towards the brighter and faster streamers.

In figure 9 an overview is given for all streamers analyzed. Discharges that (1) belong to the first half of accumulated iterations, (2) where the streamer crosses the gap, (3) have at least one branching event and (4) can be fully resolved by the algorithm are analyzed and included into the statistics, see figure 7 where the analyzed discharges are plotted in green.

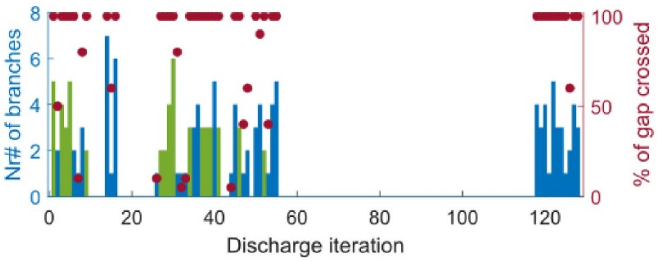

Figure 7. Imaged discharge statistics. The number of streamer branches and the percentage of the gap traversed are plotted on the left and right y-axis respectively. Note that not all discharges are imaged due to the 7.22 fps imaging rate versus the 20 pps pulsing rate. The discharges fully reconstructed are marked in green.

5.1. Categorization of branching

From the discharge tree reconstructions the branching events can be categorized accurately, relating the conditions of the event to its properties. Having information on the conditions at which a branching event occurs helps to determine the sensitivity of the underlying branching mechanisms to these conditions. Figure 10(a) shows the branching angles of all branching occurring in the analyzed discharges. The histogram in red depicts the branching angle as determined by the circular paths of the daughter streamers intersecting the parent streamer. The histogram in blue on the other hand depicts the branching angle as determined by only the triangulated detections. This means that for both daughter streamers, the first two detections along their trajectory are used to create a vector, between which the angle is calculated, see the black annotations in figure 6(b). The median branching angles are 72° and 54°, for the circular and linear methods respectively. The linear method underestimates the branching angle, since it compares the orientation of the streamer at some point after the branching. This is partially because the branching event is sampled at a finite frequency by the stroboscopic gating, so the exact moment of branching is not imaged. The circular method tries to account for this by placing the moment of branching at some point between when the streamer is considered a parent and the daughters. Additionally, directly after branching, when the resulting daughters are on their own trajectories, they repel each other, creating curved trajectories for which the branching angle at the origin seems to approach the 90°, as is expected for repelling charges. This effect is most dominant directly after the branching event, at later times the trajectories straighten and the approximation of the circular trajectories becomes worse, see especially the discrepancy between the circular trajectories and the triangulated detections near the grounded plate where they are more strongly aligned to the grounded plate, e.g. the end trajectory differences in figure 9 image 30 between the render and the green

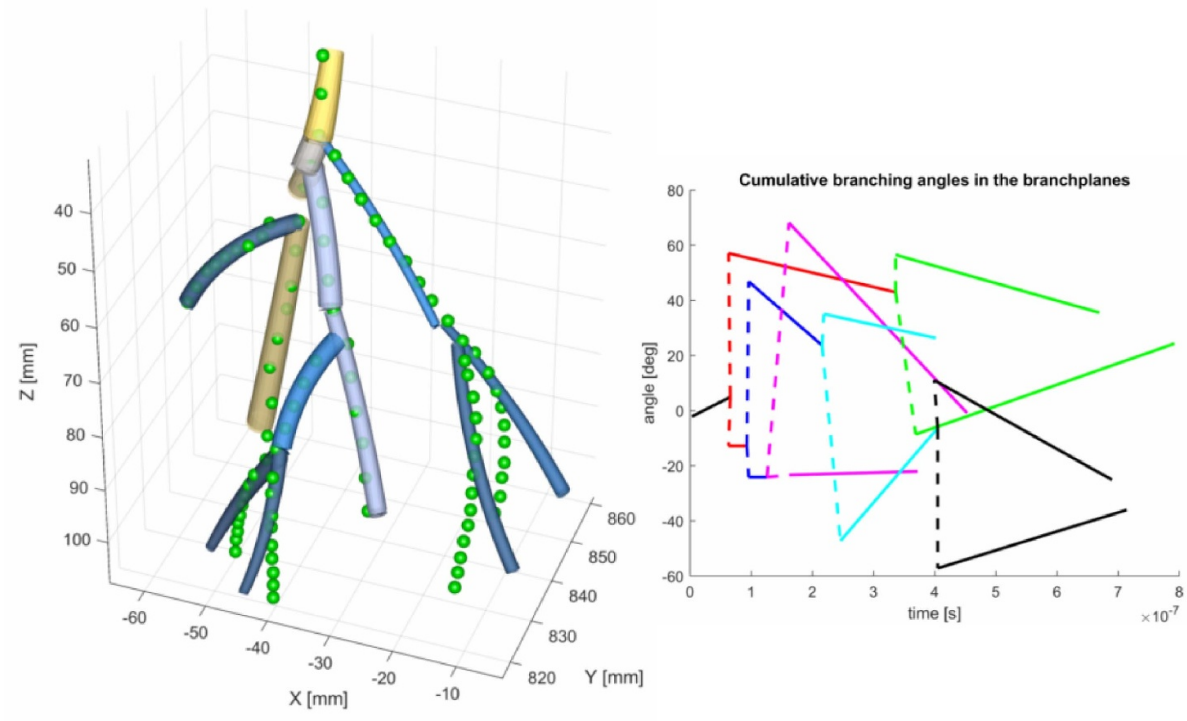

Figure 8. Streamer tree for discharge image #30, showing one of the most complex streamer trees which is still fully resolved with the described method. (a) The fitted trajectories with triangulated detections, and (b) cumulative branching angles for the successive branch planes.

dots. Nijdam *et al* [16] found an average angle for the branching streamers of 45° at 220 mbar for a point-plane electrode geometry, closer to the 54° found for the linear method in figure 10(a) and 53° of Chen *et al* [4].

In figure 10(b) the position of the branching events along the z-axis are plotted. Unsurprisingly, it shows that first branching generally occurs in the first half of the gap, and that other branching events take place later, more branches means a higher total branching probability. In the lowest 20 mm of the gap there is no more branching, as electrode effects cause a rapid connection between the streamer and the cathode plane.

Figure 10(c) indicates the likeliness of branching for all the streamer segments by expressing the ratio of propagation length between branching events and the diameter of the streamer. The diameter is averaged over the detections along each respective segment. The median distance over diameter for a streamer to branch for this experiment lies around 10. As mentioned before, Luque and Ebert [20] gives a result of about 8, while the experimental results of Briels *et al* [8] and Nijdam *et al* [16] are around 12–15. Note the difference in electrode geometry conditions for which these values are determined: Luque and Ebert [20] uses a homogenous background field, Briels *et al* [8] and Nijdam *et al* [16] use point plane geometries while in this experiment two opposing disks, one with a protruding needle, are used.

The segments are further discriminated by their occurrence along the discharge formation to clarify potential biases. The final propagation distance of the streamer towards the grounded plate never experiences branching while the shortest segments have less accurate diameter estimations and are overestimated due to the sometimes overlapping detection blobs. Segments are split into three categories, from inception to the first branching event, between branching events and the final segments which propagate to the grounded plate. The notable segments of the highest L/D bin are from the long and thin segments of discharge nr 1 and 5, see figure 9, which is something observed quite frequently in streamer discharge images captured in this experiment. These streamers can be seen as too small to branch further into smaller streamers [1, 8]. Also note, the non branching streamers are not included in this data set.

The histograms of figure 10 categorize the branching events, which follow due to an instability in the streamer head. The source of instability, whether it be stochastic photoelectrons or electron density fluctuations causing the perturbation [1, 3, 20], may be deduced from the parameters of the branching event. The branching parameters together with the segment properties give a good description of the streamer discharge morphology.

Branching of the streamers affects the space filling of ionized gas in the gaseous volume between the electrodes. Thus, where non branching streamers simply ionize a cylindrical channel between the electrodes, branching trees can cause larger, but partial, volumes of gas to be ionized. This also affects the spatially dependent electric field pulse experienced by the gas in response to the streamer. Since smaller (branched) streamers have a more localized electric field, the gas is locally excited by stronger but temporally shorter electric field pulse.

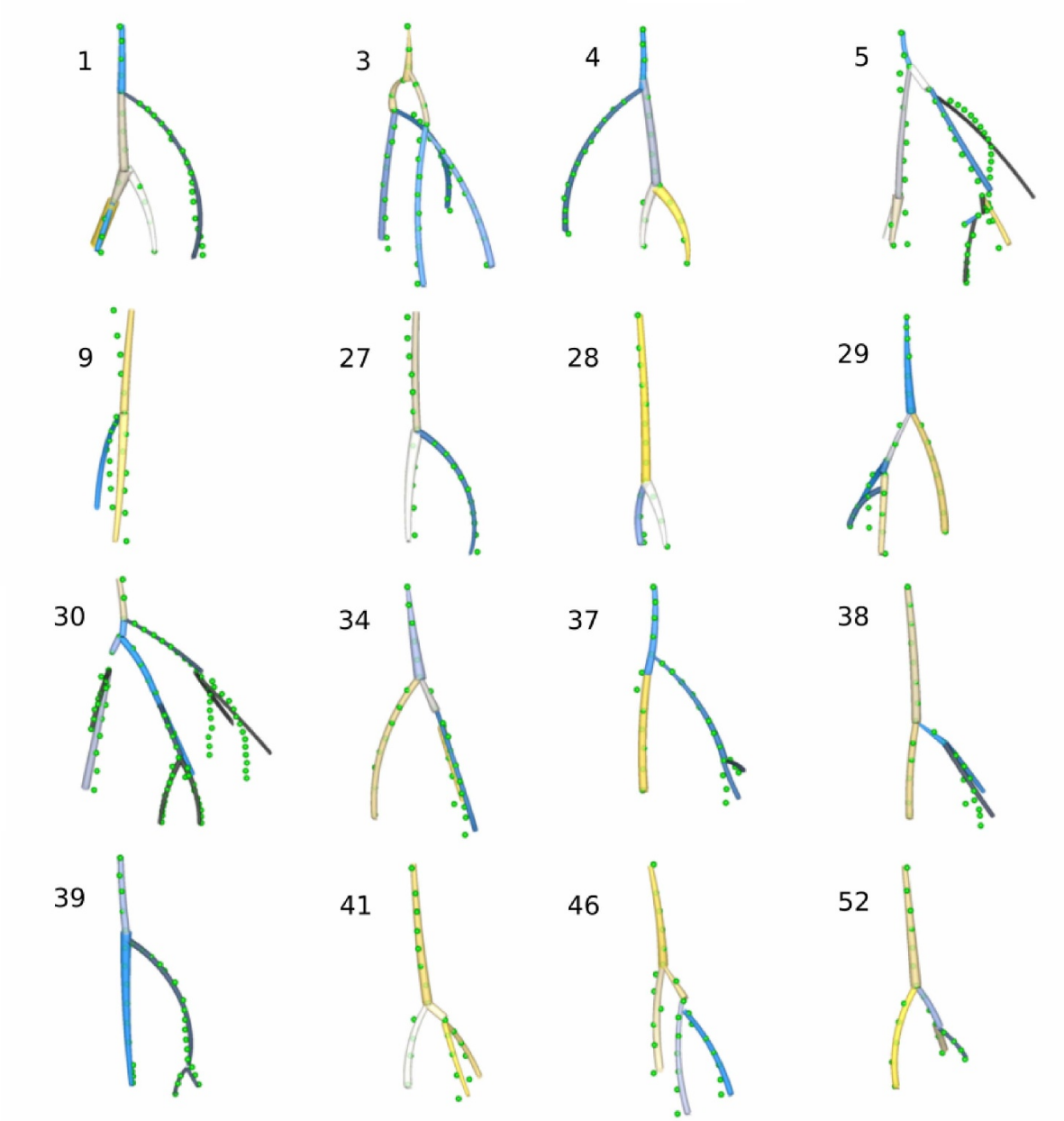

Figure 9. Overview of all analyzed discharges, showing a rendered version of the streamer together with the triangulated detections as green dots. The discharge numbers correspond to the discharges marked green in figure 7.

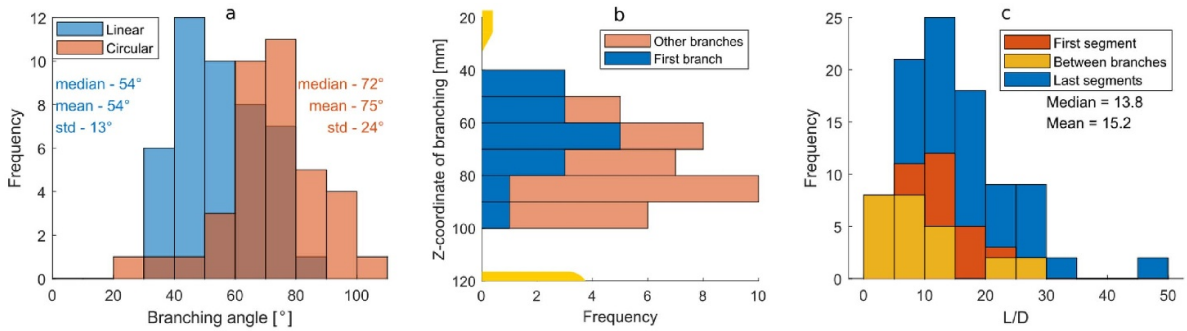

Figure 10. (a) Overlapping histograms showing the branching angles determined by the linear trajectories in blue and the circular trajectories in red. (b) The histograms show where in the discharge gap the branching took place. In blue the location of the first branching event in each discharge and the total histogram with the red bars on top show all branching occurring during the discharges. (c) Length of the segment divided by the diameter of the segment, for all 94 segments in the 16 analyzed discharges.

6. Conclusion and outlook

Imaging as a diagnostic tool for streamer images still has a lot of promising new prospects when advanced imaging and post processing techniques are applied, although it can be challenging to extract the relevant information from images.

We have developed a method which is able to extract streamer tree path morphology, velocity and diameter from stereoscopic, stroboscopic image data. It is successful for discharges with complexities up to about five branching events. This allows the analysis of large data sets, for which relevant morphological features can be compared to modelling efforts for model validation. A example of such an analysis and comparison using the experimental and processing methods described in this work can be found in Wang *et al* [12].

The reconstruction performance is directly related to the quality of the raw image. This can be improved by using a multiple camera setup, imaging the discharge from various angles with stroboscopic and single exposure gating. The imaging can be coupled to sensitive current and voltage measurements and detailed discharge inception timings, such that the shot to shot morphology can be correlated with these. All such sensory input can then be combined using a more sophisticated algorithm, based on a Kalman filter approach.

The algorithm described in this work uses the central coordinates of each detected blob to create the streamer trajectories, even the erroneous ones. The mentioned Kalman filter technique can process these detections with a probability of accuracy. Improved trajectories, and thus discharge trees can then be fitted to the detections using a streamer propagation model; a simple model predicting expected velocities, diameters and branch rates, possibly based on the experimental data itself.

The streamer discharge morphology, captured in the histograms, is very sensitive to the branching parameters. In future work, parameter scans, including pressure, voltage and gas composition can elucidate the sensitivity of the branching mechanism to these parameters.

Sophisticated knowledge of the morphological streamer discharge growth can be used to derive an electrodynamic description, from which the excited species densities can be calculated.

Data availability statement

The data that support the findings of this study are openly available at the following URL/DOI: 10.5281/zenodo.7584513 [29].

ORCID iDs

Siebe Dijcks https://orcid.org/0000-0001-7457-0215
Sander Nijdam https://orcid.org/0000-0002-1310-6942

References

[1] Nijdam S, Teunissen J and Ebert U 2020 The physics of streamer discharge phenomena *Plasma Sources Sci. Technol.* **29** 103001
[2] Luque A and Ebert U 2014 Growing discharge trees with self-consistent charge transport: the collective dynamics of streamers *New J. Phys.* **16** 013039
[3] Bagheri B and Teunissen J 2019 The effect of the stochasticity of photoionization on 3D streamer simulations *Plasma Sources Sci. Technol.* **28** 045013
[4] Chen S, Wang F, Sun Q and Zeng R 2018 Branching characteristics of positive streamers in nitrogen-oxygen gas mixtures *IEEE Trans. Dielectr. Electr. Insul.* **25** 1128–34
[5] Ebert U *et al* 2010 Multiple scales in streamer discharges, with an emphasis on moving boundary approximations *Nonlinearity* **24** C1–C26
[6] Adamovich I *et al* 2022 The 2022 plasma roadmap: low temperature plasma science and technology *J. Phys. D: Appl. Phys.* **55** 373001
[7] Pancheshnyi S, Nudnova M and Starikovskii A 2005 Development of a cathode-directed streamer discharge in air at different pressures: experiment and comparison with direct numerical simulation *Phys. Rev.* E **71** 016407
[8] Briels T M P, Kos J, Winands G J J, van Veldhuizen E M and Ebert U 2008 Positive and negative streamers in ambient air: measuring diameter, velocity and dissipated energy *J. Phys. D: Appl. Phys.* **41** 234004
[9] Gallimberti I 1972 A computer model for streamer propagation *J. Phys. D: Appl. Phys.* **5** 2179–89
[10] Marskar R 2020 3D fluid modeling of positive streamer discharges in air with stochastic photoionization *Plasma Sources Sci. Technol.* **29** 055007
[11] Teunissen J and Ebert U 2017 Simulating streamer discharges in 3D with the parallel adaptive afivo framework *J. Phys. D: Appl. Phys.* **50** 474001
[12] Wang Z, Dijcks S, Guo Y, van der Leegte M, Sun A, Ebert U, Nijdam S and Teunissen J 2022 Quantitative prediction of streamer discharge branching in air (arXiv:2208.07279)
[13] Li X, Dijcks S, Nijdam S, Sun A, Ebert U and Teunissen J 2021 Comparing simulations and experiments of positive streamers in air: steps toward model validation *Plasma Sources Sci. Technol.* **30** 095002
[14] Šimek M 2014 Optical diagnostics of streamer discharges in atmospheric gases *J. Phys. D: Appl. Phys.* **47** 463001
[15] Trienekens D J M, Nijdam S and Ebert U 2014 Stroboscopic images of streamers through air and over dielectric surfaces *IEEE Trans. Plasma Sci.* **42** 2400–1
[16] Nijdam S, Moerman J S, Briels T M P, van Veldhuizen E M and Ebert U 2008 Stereo-photography of streamers in air *Appl. Phys. Lett.* **92** 101502
[17] Raizer Y P 2011 *Gas Discharge Physics* (Berlin: Springer)
[18] Babaeva N Y and Naidis G V 2021 Universal nature and specific features of streamers in various dielectric media *J. Phys. D: Appl. Phys.* **54** 223002
[19] Briels T M P, van Veldhuizen E M and Ebert U 2008 Positive streamers in air and nitrogen of varying density: experiments on similarity laws *J. Phys. D: Appl. Phys.* **41** 234008
[20] Luque A and Ebert U 2011 Electron density fluctuations accelerate the branching of positive streamer discharges in air *Phys. Rev.* E **84** 046411
[21] Ichiki R, Kanazawa S, Tomokiyo K, Akamine S, Kocik M and Mizeraczyk J 2012 Investigation of three-dimensional characteristics of underwater streamer discharges *Jpn. J. Appl. Phys.* **51** 106101

[22] Seeger M, Votteler T, Ekeberg J, Pancheshnyi S and Sanchez L 2018 Streamer and leader breakdown in air at atmospheric pressure in strongly non-uniform fields in gaps less than one metre *IEEE Trans. Dielectr. Electr. Insul.* **25** 2147–56

[23] Naidis G V 2009 Positive and negative streamers in air: velocity-diameter relation *Phys. Rev.* E **79** 057401

[24] Dijcks S, Kusýn L, Janssen J, Bílek P, Nijdam S and Hoder T 2022 High-resolution electric field and temperature distributions in positive streamers (arXiv:2212.11157)

[25] Lloyd S 1982 Least squares quantization in PCM *IEEE Trans. Inf. Theory* **28** 129–37

[26] Hartley R and Zisserman A 2004 *Multiple View Geometry in Computer Vision* (Cambridge: Cambridge University Press)

[27] Chen S, Heijmans L C J, Zeng R, Nijdam S and Ebert U 2015 Nanosecond repetitively pulsed discharges in N_2–O_2 mixtures: inception cloud and streamer emergence *J. Phys. D: Appl. Phys.* **48** 175201

[28] Mirpour S, Martinez A, Teunissen J, Ebert U and Nijdam S 2020 Distribution of inception times in repetitive pulsed discharges in synthetic air *Plasma Sources Sci. Technol.* **29** 115010

[29] Siebe D, Sander N and Martijn L V der 2023 Imaging and reconstruction of positive streamer discharge tree structures (available at: https://zenodo.org/record/7584513)